Optical Spectrum of the compact Planetary Nebula IC 5117

Siek Hyung[1], Lawrence H. Aller[2], Walter A. Feibelman[3], Seong-Jae Lee[4]

[1]*Korea Astronomy Observatory, 61-1 Whaam-dong, Yusong-gu, TaeJon 305-348, Korea*
[2]*Physics and Astronomy Department, University of California, Los Angeles, California 90095, USA*
[3]*Laboratory for Astronomy and Solar Physics, Code 684.1, NASA Goddard Space Flight Center, Greenbelt, MD 20771, USA*
[4]*Dept. of Astronomy and Space Science, Chungnam National University, TaeJon 305-764, Korea*

ABSTRACT

High resolution spectroscopic data of the very compact planetary nebula IC 5117 are obtained in the optical wavelengths, 3700Å – 10 050Å, with the Hamilton Echelle Spectrograph at Lick Observatory, and which have been analyzed along with the International Ultraviolet Explorer (*IUE*) UV archive data. Although a diagnostic diagram shows significant density and temperature fluctuations, our analysis indicates that the nebular gas may be represented by a homogeneous shell of extremely high density gas, $N_\epsilon \sim 90\,000$ cm^{-3}. The average electron temperatures, e.g. indicated by the [O III] diagnostics, are around 12 000 K. We construct a photoionization model to represent most of the observed line intensities, and the physical condition of this compact nebulosity. Based on the semi-empirical ionization correction approach, and model indications, we derived the elemental abundances: He, C, N, O, Ne, and Ar appear to be normal or marginally depleted compared to the average planetary nebula, while the remaining elements, S, Cl, and K appear to be enhanced. IC 5117 is perhaps a very young compact planetary nebula, slightly more evolved than the other well-known compact planetary nebula IC 4997. The central stellar temperature is likely to be around 120 000 K, evolved from a C-rich AGB progenitor.

Subject headings: ISM: abundances: planetary nebulae: individual (IC 5117)

1. Introduction

IC 5117 is a very young compact planetary nebula (PN) with molecular emission. CO often succeeds in forming and surviving within the envelopes of more massive nebulae (Mamon et al. 1988). Gussie & Taylor (1995) observed both H I and CO envelopes in IC 5117: they suggested that the H I is formed within a photodissociation region inside a larger molecular envelope and

exterior to the ionized gas. The spatial distributions of the CO and H I are unknown, so a spatial comparison between the molecular and atomic components is impossible.

In the radio continuum and H92α study by Miranda et al. (1995), strong variations of the radial velocity were detected on angular scales of $\simeq$0.3″, and a kinematical age of $\simeq$350 yr was inferred (for an assumed distance of 3 kpc). They also reported variations of the electron temperature and density on scales of $\simeq$0.4″. The high brightness temperature in radio frequencies, which is indicative of distance-independent density information, had been noted in earlier studies, e.g. the VLA 6-cm continuum observation by Zhang (1995). IC 5117 is known to be one of the youngest PNe. It is unknown whether or not the observed neutral gas is causally connected with the nebula, and it is not clear whether the ionized shell in IC 5117 grows at the expense of an outer neutral shell.

With the Image Tube Scanner (ITS), Aller and Czyzak (1979, hereafter AC79) secured a number spectral lines, but the wavelength dispersion was relatively poor compared with the currently available high dispersion spectral data obtained with charge coupled devices (CCDs) used with, e.g. an echelle spectrograph. Thus, it would be better to find the abundances from recently available high quality data, with the help of appropriate models. We revisited IC 5117 to secure a high dispersion optical spectrum, from 3700 to 10 050Å, with the Hamilton Echelle Spectrograph (HES) at Lick Observatory. We compared the optical spectrum from the HES with that of the ITS, and we also re-measured the *IUE* archive data in the UV region. For these relatively complete wavelength coverage data, we obtain the diagnostics from which we compute the ionic concentrations. With the help of a reliable photoionization model, we try to fit the observed optical emission lines and other wavelength region archival data to determine the physical condition of IC 5117 which best represents the diagnostics and the nebular gas. Finally, we determine the abundances of IC 5117, compare these with the solar and average nebular abundance, and discuss briefly the evolutionary status. Table 1 gives some basic data for IC 5117, and useful references.

2. Observations

There are 4 *IUE* spectra available for IC 5117: SWP 25835 (30min, 1985 May 2), SWP 31825 (150min, 1987 Sep 11), LWP 05883 (30min, 1985 May 2), and LWP 05884 (295min, 1985 May 2). All these spectra are low dispersion, and were taken through the large (10″ × 23″ oval) entrance aperture of the *IUE* cameras. The *IUE* data were reduced with the latest *IUE* reduction techniques at the Goddard Space Flight Center (GSFC), i.e. with the NEWSIPS routine. The apparent size of IC 5117 is small enough to fit into the large entrance aperture, so that the *IUE*-observed emission comes from the entire nebula. We measured the spectrum from two long exposures, i.e. SWP 31825 and LWP 05884, and ignored the other relatively poor quality exposures. These emission line measurements are given in Table 2. Successive columns of Table 2 give the observed and laboratory wavelengths, the ion, Seaton's extinction parameter, k_λ, the extinction corrected intensity with E(B-V) = 0.88 [relative to I(Hβ) = 100], and the measured flux in units of 10^{-14} erg cm^{-2} s^{-1} (note that the flux unit is one order of magnitude lower than those of the other

well-known PNe investigated in our previous studies!). In Fig. 1 we plot the combined *IUE* SWP + LWP spectra in the wavelength range from 1200 to 3250 $\AA$ (the extinction correction was not applied). All spectra were smoothed with a 3-point running average.

For the near UV region (from the limit of the Balmer series down to the atmospheric cutoff near 3100Å), we refer to the high sensitivity 'green' tube (ITS) archive data by Likkel and Aller (1986, hereafter LA86). Table 3 gives the near UV measurements by Likkel (private communication). The first column gives the measured wavelength from LA86; the second column gives the laboratory identification; the extinction parameter, k_λ, is listed in column (3). Column (4) gives the derived intensity, corrected for interstellar extinction; column (5) gives the measured flux data secured by LA86 from the green tube ITS observations. Here, the intensities are given on the scale of I(Hβ) = 100, after applying the extinction correction (with $C = 1.29$), while the fluxes are in units of 10^{-14}erg cm^{-2} s^{-1}. 'B' in the last column denotes Bowen fluorescent O III lines, which had been investigated by LA86. In this region fall lines of He I and O III, but no lines of He II, O IV, [Ne III] (auroral-type), [Ne V], and [Na IV]. We quoted the [O II]3727 lines in order to compare with the HES spectral measurements. In Table 3, and in the following Tables, we have given 1 or 2 more significant figures than the data justify, to avoid round-off errors.

The optical region observations were all obtained with the HES at the Coudé focus of the 3 m Shane telescope of Lick Observatory, on 1995 August 18. We obtained two exposures, 120 minutes and 5 minutes, on IC 5117. The sky was very clear during our observations, and seeing was less than $\sim 1.5''$. The spectroscopic slit employed was 640 μm in width, which amounted to $\sim 1.2''$ in image size at the Coudé focus. For this slit width, the limiting resolution on the CCD chip was about 2 pixels which amounted to 0.05$\AA$ wavelength dispersion at 3600$\AA$, and increased to 0.15$\AA$ at 8850$\AA$. The slit length of $4''$ was chosen to avoid confusion of successive echelle orders.

For spectral calibration, we took exposures of a Th-Ar arc lamp to set the wavelength dispersion scale; a dome-quartz lamp to fix a flat field which allowed us to correct for pixel to pixel sensitivity fluctuations; and finally exposures on two standard stars of known energy distribution, i.e. M39-23 (chosen for the blue wavelength region flux calibration) and Eta Ursa Majoris (for the red wavelength region flux calibration). The absolute fluxes of these two standard stars were available from Mr. Remington Stone (private communication, 1995). We used a large 2048×2048 pixel CCD, which covered the whole HES echelle pattern. The reduction procedures are described in Hyung (1994). We present the HES results in Table 4. A large number of optical lines were measured. Successive columns give: the measured wavelength (corrected for radial velocity), the wavelength of the most probable identification, the ion, the multiplet number from Moore's tabulations (1974, 1993), and Seaton's extinction parameter, k_λ. We found the radial velocity of IC 5117 to be -38.7 ± 0.7 km s^{-1}, while Acker et al. (1992) quote -26.1 ± 1.3 km s^{-1}. The discrepancy may be caused by some of the selected lines being different between these two analyses. We obtained our value from a comparison of the observed wavelengths of the strong lines (I > 1.0) with the laboratory wavelengths, using the least squares method; the central wavelengths of the emission profile were converted to heliocentric radial velocity (+6.5 km s^{-1}), following the method of Herrick (1935).

The 6th column gives the HES intensity on the scale I(4861) = 100.0, corrected for interstellar extinction, with an extinction coefficient C = log I(Hβ)/F(β) = 1.40±0.13 found from Balmer line ratios, such as $F(H\alpha)/F(H\beta)$, and from a comparison of Balmer and Paschen lines of the same upper quantum number: n = 10, 12, 14, & 16, i.e. 9015Å vs. 3798Å and 8750Å vs. 3750Å etc; this is different from the value of C=1.29 used for the UV region *IUE* and near-UV region ITS data. The higher value of C for the HES data is probably an overestimation due to an observational or data reduction error involving the instrumental and atmospheric response functions. The 7th column presents the HES flux on the scale F(4861) = 100.0, while the last column lists the formal root mean square (RMS) % error, as deduced from the internal disagreement of measurements made with different CCD chip position settings (whenever two or more measurements are available).

The spectrum of IC 5117 was not divided by that of the standard star in order to take out the 1st order effects of the atmosphere. However, since the HES produces a high dispersion spectrum, one can clearly tell which lines are severely affected by the telluric absorption. The errors increase towards the ends of each order, and with the underlying noise. Lines affected by "bleeding" from a strong line in a nearby order may be seriously impacted. By taking a graded series of exposures, this difficulty can often be overcome. Several procedures are available for estimating the accuracy of the measurements. By comparing data obtained on different nights, and with different chip positions, we can assess the effect of guiding errors, influence (if any) of position in the field, and of the response function. On the absolute flux scale Flux(Hβ) = 100, statistics show that lines weaker than I = 1.0 will have errors of 15% to 40%; for lines in the range 1.0 $\leq$ I $\leq$ 10.0, errors fall in the interval 7% to 20%; for stronger lines, we estimate errors of 3% to 10%. In Fig. 2, we present three reduced spectral scans to show the quality of our HES data.

3. Diagnostics

Numerous lines, including many strategically important diagnostic lines especially useful for nebular diagnostic and abundance determination, are observed in the optical spectrum of IC 5117. All of the listed optical lines in Table 4 were resolved, but their line profiles mostly do not show a double peak feature. However, we were able to separate the double component for the case of strongly measured low excitation lines, i.e. [N II]6584, using the STARLINK/DIPSO tool. The derived expansion velocity from the [N II] line profiles is about 11.4 km s^{-1}, while expansion velocities quoted by Acker et al. (1992), i.e. 21.5 km s^{-1} ([N II]) and 16.5 km s^{-1} ([O III]), are larger than our derivation. The following ions are detected in the HES spectrum of IC 5117: H, He I, He II, C I, [C I], C II, C III, C IV, N I, [N I], N II, [N II], N III, [O I], O II, [O II], O III, [O III], Ne I, [Ne III], [Ne IV], S I, S II, [S II], [S III], [Cl II], [Cl III], [Cl IV], [Ar III], [Ar IV], [Ar V], [K III], [K IV], [Ca VII]?, Mn I?, [Mn V], [P I], [F II]?, [Fe II], [Fe III], [Fe VI], and [Fe VII]. UV and near-UV lines detected are as follows: He I, He II, C II], C III], C IV, [N II], N III], N IV, N V?, [O II], O III, O III], [Ne IV], [Ne V], Si II], Si III], Ar II, Na IV. Diagnostic line ratios suitable for fixing the electron densities and temperatures, (N_ϵ,T$_\epsilon$), are listed in Table 5, and Fig. 3 shows

the diagnostics based on those line ratios involving equivalent p^2 and p^4 electrons. Electronic collision strengths involving the plasma and nebular diagnostics are constantly updated from the most recently available data, as in our previous investigations, e.g. Hyung et al. (2001).

Diagnostics of [Cl III], [S II], [N II], [Ar III], and [Cl IV] intersect near a single point, i.e. log N_ϵ = 4.6 and $T_\epsilon \sim$ 12 000 K. However, the electron temperatures, especially indicated by the [O III] lines, are extremely high, for the above density, log N_ϵ = 4.6. According to Aller & Liller (1968: see their Fig. 1), the He II4686/Hβ ratio $\sim$ 0.1 implies that this PN has excitation class 6. The other line ratio I(λ3726+3729)/I(λ4959) also indicates excitation class 6. Providing this PN is in a medium excitation class, we may be able to choose another point at a much higher density log N_ϵ = 4.95 (corresponding to N_ϵ = 90 000 cm^{-3}) as a representative physical condition. This latter point implies relatively lower electron temperatures, e.g. $T_\epsilon \simeq$ 11 800 K from the [O III] [4959+5007]/4363 ratio, and $T_\epsilon \sim$ 11 500 K from [Ar III] and [Cl IV]. In this case, the electron temperatures for the lower excitation line-emitting strata, e.g. [S II], [N II], would also be lower, e.g. T_ϵ([N II]) $\sim$ 9 000 K. For [S III] and [O II], we still find very high electron temperatures, T_ϵ $\sim$ 14 500 K. Model investigations presented in the following section also seem to indicate physical conditions in favor of the relatively high density nebula gas. In fact, the nebula itself may consist of many inhomogeneous blobs and filaments, where some effects of T_ϵ fluctuation, considerably greater than that predicted by our photoionization models, may exist (see Peimbert et al. 1995).

With the forbidden lines involving p^3 electrons, one can also obtain diagnostics for both density and temperature at the same time (see Keenan et al. 2000; 1999; 1997; 1996). (1) [O II]: λ3729/λ3726 vs. λ7320/(λ3726 + λ3729) gives (T_ϵ, log N_ϵ) = (12 500 K, 4.9), while λ3729/λ3726 vs. λ7330/(λ3726 + λ3729) gives (15 000 K, 4.8). Similarly, (2) [Ar IV]: λ4711/λ4740 vs. λ7263/(λ4711 + λ4740) gives (T_ϵ, log N_ϵ) = (18 000 K, 4.9); (3) [S II]: λ6716/λ6731 vs. λ4068/(λ6716 + λ6731) gives (T_ϵ, log N_ϵ) = (15 000 K, 4.4), while λ6716/λ6731 vs. λ4076/(λ6716 + λ6731) gives (17 500 K, 4.4). (4) [Cl III]: λ5518/λ5538 vs. λ8434/(λ5518 + λ5538) gives (T_ϵ, log N_ϵ) = (20 000 K, 4.6). The electron temperatures indicated by these p^3 diagnostics are probably subject to a relatively large error (due to the crowding of temperature diagnostic lines, see e.g. Figs. 2 & 3 of Keenan et al. 1996), so the temperature determination from the p^3 diagnostics may incur a large error. On the other hand, the density diagnostics appear to be quite useful. For most ions, the electron densities indicated by the p^3 diagnostic lines are N_ϵ = 90 000 cm^{-3} (log N_ϵ = 4.9), but for some other ions, e.g. [S II] and [Cl III], lower values are indicated, i.e. $N_\epsilon \sim$ 30 000 – 40 000 cm^{-3} (log N_ϵ = 4.4 – 4.6). The neutral lines, such as [N I], must be formed in a region of very low density, $N_\epsilon \sim$ 6300 cm^{-3}.

4. Theoretical Models

To construct a theoretical model, one must know the spectral energy distribution (SED) of the central star of the planetary nebula (CSPN), or else certain other properties of the CSPN. The SED of the CSPN can be calculated by employing Hubeny's model atmosphere (1988). The CSPN of IC

5117 is classified as a Wolf-Rayet (WR) star. Köppen & Tarafdar (1978) derived the temperature of the CSPN, i.e. 64 000 K from the [O^{2+}/O^{+} ratio] and 67 000 K from the [He(4686)/Hβ ratio], while Zhang & Kwok (1992) derived a similar CSPN temperature of 56 700 K, from their model fitting to the IR lines, and to the observed continuum SED. We directly applied Hubeny's theoretical model atmospheres based on some of the selected properties of the CSPN (i.e. T_{eff}, stellar radius, log g), to the photo-ionization modeling, until it gave a correct level of nebular excitation (using the energy-balance method and the Zanstra method), and the correct electron temperatures. From our trials, we found that model atmospheres with relatively high temperatures are suitable for the CSPN, e.g. T_{eff} = 120 000 K. The model predictions with lower temperatures for the CSPN, e.g. $T_{eff} \sim$ 85 000 K, seem to fit some of lines, but the predicted electron temperatures are in general too low.

Details of parameters adopted in our model are given in Table 6 (see Model B in Table 7). Acker et al. (1992) quoted various distance determinations to IC 5117, which together show a large scatter, from 0.8 to 7.78 kpc. To a first approximation, the correct value of the distance to the PN is not critical in fitting the line intensities. However, we must narrow it down to a reasonable range, since only the correct distance would give an appropriate physical scale for both the CSPN and the PN. We adopted an intermediate value of ~3.0 kpc. Thus, for a distance of 3.0 kpc, we refined the model, scaling the CSPN properties and model geometry to reproduce the absolute Hβ flux to within observational errors.

The absolute intrinsic Hβ flux is F_{corr}(Hβ) = 8.33 – 10.7×10^{-11}[written as (−11), henceforth] erg cm^{-2} s^{-1} for C = 1.29 – 1.4 (from the observed Hβ flux, F(Hβ) = 4.27(−12) erg cm^{-2} s^{-1}, see Tables 1 and 6). The model predicts F(Hβ) = 9.67(-11) erg cm^{-2} s^{-1}. The observed visual magnitude is m_v = 16.7, and accordingly the intrinsic visual magnitude V_{obs} = 14.0 using E_{B-V} = 0.88 (the corresponding total extinction A_v is here taken as 3.1E_{B-V}). The model predictions give values that are about one magnitude lower than the observed ones: V_{pred} = 15.1 and B_{pred} = 14.9. In addition, the model cannot match the observed nebular size: the outer radius of the model shell is density bounded, and its projected angular scale on the sky is slightly larger than the observed one.

The CSPN energy distribution used in the model has T_{eff} = 120 000 K and log g = 8.5, with He/H = 0.1, and with a nebular heavy element distribution in the central star. The nebula is assumed to be a homogeneous shell with N_H = 80 000 cm^{-3}. No filling factor is introduced in the shell gas. We assume a central star radius of R_* = 0.06$R_\odot$ and, as a result, L_* = 670 $L_\odot$. A significant amount of the energy is emitted in the far-infrared due to the thermal emission of dust grains (Zhang & Kwok 1992). This relatively large amount of dust may have some effects on the UV emission lines, especially the resonance lines. We, however, used a small amount for the dust to gas ratio, M_{dust}/M_{gas} = 0.001, so the prediction for some of UV region resonance lines would not be expected to be good.

We did not employ a composite model geometry with an inhomogeneity in the nebular gas,

but we constructed two models, 1) model A with N_H =40 000 cm^{-3}, and 2) model B with a higher density in the shell, i.e. N_H =80 000 cm^{-3}. The chemical abundances adopted in the above models are slightly different. Although model A and model B produce a fairly good fit to the lines, the former model has a serious problem with some of diagnostically important lines, e.g. [O II]7321/7332. As indicated in Fig. 3, the higher density model would be desirable. Thus, we prefer the latter model with N_H =80 000 cm^{-3} (giving an electron density of N_ϵ =90 000 cm^{-3}), which gives a better prediction for most of lines, including the [O II] lines. Table 7 compares the observed and predicted intensities. Intensities from the ITS by AC79, and from our HES + *IUE* Archive data, are given in columns (3) and (4), respectively, while columns (5) and (6) list the predicted intensities. All of the values are on a scale of I(Hβ) = 100.

The following discussion is based on model B. For most ions, fairly reasonable agreement between the observed and predicted intensities is achieved, but in some cases, especially [Ar V], we find a glaringly large discrepancy. The agreement for He I and He II seems fine. As usual, in predicting He lines, we corrected for collisionally excited contributions. The predictions for C seem fine, except for the recombination C II λ4267 line, and C IV. In fact, Model A is favored by the observations of C IV. Predictions for the ions of N, O, Ne, S, and Cl seem generally successful. The [S II]6717/6731 lines have a problem. However, the agreement for other sulfur lines appears fine. Although the [S IV] IR line available from Beck et al. (1981) involves an uncertain extinction correction, we were also able to fit this line. Here, the lower density model A seems to fit the [S II] lines better. Rare elements like Si and K are all represented by single ionization stages: silicon by Si III], and potassium by [K IV]. Hence, agreement for these ions can be assured, and the abundances of these elements can be found by the model.

The electron temperatures indicated by the diagnostics are T$_\epsilon$ = 12 000–14 500 K, 11 800 K and 11 500 K, for [O II], [O III], and [Ar III], respectively. However, model B predicts T$_\epsilon$ = 12 500 K, 11 800 K and 12 300 K, respectively. Thus, the relatively higher temperatures indicated by the [O II] diagnostic, in contrast to the average electron temperature deduced from [O III], seem to be confirmed by the model. The model obviously cannot be consistent with the large scatter indicated by other diagnostics. There also appear to be some observational errors involved: for example, the diagnostics indicate a very low temperature for the [N II] lines, but the model did not predict such a relatively low temperature, i.e. T$_\epsilon$ < 11 000 K ([N II]: see Fig. 3) vs. 12 600 K (model B). Since our model structures are basically simple homogeneous shells, they do not admit a point to point fluctuation of N_ϵ. Note also that our photoionization models require a higher effective temperature for the CSPN, contrary to the derivations by Zhang & Kwok (1992) or Köppen & Tarafdar (1978). The CSPN temperature of IC 5117 is likely to be high, around T$_{eff}$ = 120 000 K.

We tried to simplify the problem by choosing a single diagnostic point to represent the physical conditions of PN. As a result, our model predicts the central star visual brightness as being one magnitude dimmer than observed, and, in addition, the predicted nebular size is slightly overestimated. This contradiction may disappear if we employ a WR-type model atmosphere for the CSPN (see Hyung et al. 2000).

5. Abundances

5.1. Ionic Concentrations

With the appropriate electron temperature, T_ϵ, and electron density, N_ϵ, we are now able to obtain the ionic concentrations by well-known formulae (see e.g. Aller 1984), updated with the most recent and reliable values of atomic constants. Table 8 presents the ionic concentration calculated from the interstellar extinction-corrected intensities, i.e. the UV region *IUE* and optical HES data listed in Tables 2 and 4. Successive columns present: ion involved, wavelength, intensity, and the values of $N(\mathrm{ion})/N(\mathrm{H}^+)$. In the last column, the summations of the ionic concentrations are obtained via weighting by the line intensities. In the case where the line measurements are uncertain or too weak, the results are discarded. For the choice of electron temperature and density in calculating each ionic concentration, we do not use all of the details discussed in Section 3. Instead, we applied a single representative diagnostic electron temperature and density to simplify the problem. As discussed earlier in Section 3 and in Fig. 3, there are two probable diagnostic points which may be suitable for our purpose, i.e. a) $N_\epsilon \sim 40\,000$ cm^{-3} and $T_\epsilon \sim 13\,000$ K; and b) $N_\epsilon \sim 90\,000$ cm^{-3} and $T_\epsilon = 12\,000$ K. If we adopt the former as the physical state of IC 5117, we find a large discordance in derived ionic concentrations in some ions. For example, the [O II] ionic concentration found by λ3727,3729 is only 1/4 times that by λ7320,7330. However, if we adopt the latter higher density case as a physical condition, the disagreement becomes smaller (See Table 8). The physical condition of $N_\epsilon = 90\,000$ cm^{-3} and $T_\epsilon = 12\,000$ K, which has been discussed in previous sections, appears to be more appropriate than the other lower density.

We found the ionic concentrations for both He I and He II. The latter is about 10% of the former. The combined total is lower than the previous result found in the literature (see Section 5.2). For some ions such as carbon and silicon, the optical data are unavailable, forcing us to rely solely on the *IUE* measurements. Virtually all of the C ions are accounted for by (C^+, C^{2+}, C^{3+}), and in fact mainly by (C^{2+}); here, as usual, ionic concentrations of C^+, C^{2+} and C^{3+} are derived from the UV lines, assumed to be collisionally excited. Similarly, the summation of oxygen ionic concentrations can be found from O^+ and O^{2+}. The O^{2+} ionic concentration obtained from the *IUE* O III] 1661/1666 is slightly higher than those from the optical [O III] lines. In this case, we ignored the *IUE* lines because of the relatively weak line intensities. Ionic concentrations for neon are available for (Ne^{2+}, Ne^{3+}) from the HES and *IUE*, respectively. The Ne^{3+} ionic concentration obtained from the weakly detected *IUE* line is about 25% of that found from the optical lines. For sulfur, we were able to calculate three ionic concentrations (S^+, S^{2+}, S^{3+}). The first two concentrations are measured from our HES data, while the S^{3+} concentration is based on the line intensity measured by Beck et al. (1981). Argon is mostly represented by Ar^{2+} and Ar^{3+}, with a weak contribution from Ar^{4+}. For chlorine, two ionic concentrations, Cl^{2+} and Cl^{3+}, are available, but the theoretical model indicates a fairly large contribution, i.e. ~50% from Cl^{4+} (see section 5.2). We are also able to find the ionic concentration for other rare elements. For example, potassium and silicon are represented by single ions, [K IV] and [Si III].

5.2. Abundance Determinations

To determine the abundance of IC 5117, we used two methods: 1) the Ionization Correction Factors (ICF's) method, coupled with the derivation of ionic concentrations as described in Section 5.1, and 2) models. The latter method is to use the best model available, e.g. as described in Section 4, with adopted model abundances; while the former method calculates the fractional ionic concentration for each ionic stage, and uses the ICF's suggested by the model for the unobserved ionic stages.

The elemental abundances (relative to $N(H^+)$ of IC 5117 are given in Table 9. The second column of this table lists the $\Sigma N(\mathrm{ion})/N(H^+)$ from Table 8, and the 3rd column lists the ICF obtained from the theoretical model in section 4. The 4th column gives the ICF abundance, $N(\mathrm{ICF})$, obtained from the ionic concentration by applying the ICF's for the unobserved ionic stages, i.e. by multiplying the 2nd column by the 3rd one. The 5th column gives the model abundances, $N(\mathrm{model})$, adopted from model B; the 6th column gives the logarithmic difference, i.e. $\triangle = \log N(\mathrm{ICF}) - \log N(\mathrm{Model})$, which is relatively small ($|\triangle| << 0.10$) for most elements. The 7th column gives the recommended abundance for IC 5117, while the 8th column lists the previous estimation for IC 5117 by Aller and Czyzak (1983). The last two columns list the 'average' PN abundance found by Aller and Czyzak (1983, AC83) and by Kingsburgh and Barlow (1984B), and the solar abundance by Grevesse and Noels (1993).

Both the ICF and model results are in good accord, and the abundances derived seem reasonable accurate. However, the current results are quite different from the AC79 result for C, Ne, and K. Rudy et al. (2001) recently measured the near-infrared spectrum from 0.8 to 2.5 μm. They found He/H $\sim$ 0.113, similar to the AC83 result, while our derivation produces a 10% lower value, at about the solar abundance, i.e. He/H $\sim$ 0.1. This difference may be due to the density employed in the assumed physical conditions. To fit the helium lines with the lower gas density in the shell, we need to increase the helium abundance. Our result, which is based on a relatively good photoionization model, is perhaps more accurate than that from AC83, because of the higher quality data, and improved model.

For three elements, C, N and Ar, there are big discrepancies between the ICF and model results, $|\triangle| \sim 0.1$. The model cannot fit the C IV lines, so we adopt the carbon abundance, close to the ICF method, i.e. C/H $\simeq$ 5.0(-4). Our derived C/H value is lower than AC83 value by a factor of two, i.e. 8.9(-4) from AC83. Since the abundance derived here is for a gas phase, some carbon may be tied up in grains. Based on our derivation, we suggest that the carbon abundance is likely to be close to the solar but depleted relative to the average PN. Comparing our result with AC83 for other elements, we note that there exists a large discrepancy in Ne and K. For other elements, our abundances are in accord with AC83: our derived abundances are slightly less than those of AC83 in S and Ar, though the opposite is true for Cl and K.

The current derivation of N and O abundances agree with those of AC83, i.e. N/H $\sim$ 1.3(-4) and O/H $\sim$ 3.8(-4). Thus, these are close to the average PN, but less abundant than solar.

Similarly, both Ne and Ar abundances appear close to the average PN value. We obtained Ne/H $\sim$ 6.5(-5), vs. 9.3(-5) from AC83. We derived the sulfur abundance, S/H $\sim$ 8.9(-6), 25% lower than in AC83. Rudy et al. (2001) found an even lower value, 7.5(-6). We derived a chlorine abundance of 1.85(-7), 30% higher than AC83 value, which is slightly less abundant than the average PN, but lower than solar.

6. Conclusion

We constructed a nebular model for IC 5117 based on the diagnostic information, and found the abundances in this PN. These were compared with those from AC83, and also with the average PN. For He, C, and K, we found a factor of 2 difference from AC83. We believe our result is substantially improved over the previous determination by AC83, due to higher quality data and a better theoretical model employed. Our study suggests the C/H, Ne/H, and Ar/H ratios are lower than the average PN. However, we found no evidence of metal deficiency in other elements: the He/H, N/H, O/H, and Cl/H ratios are close to the average PN. Only Si involves a large ICF.

If the assumed distance to the PN IC 5117 is correct, the employed CSPN temperature and luminosity should give us a CSPN mass. Taking L($\star$) and T($\star$) at their face values (see Table 6) and utilizing Schönberner's (1983) evolutionary tracks, we derive a CSPN mass of about 0.60 $M_{\odot}$. In addition, these tracts suggest a corresponding age of about 7000 years, as evolved from an AGB progenitor. The AGB must have been a C-rich star, i.e. C/O ratio greater than 1. The central star must have been slightly more massive than our Sun on its main sequence phase. CO emission is commonly observed in PNe of Peimbert's Type 1 or Greig's Class B (Greig 1972; Huggins & Healy 1989). However, the chemical abundances in IC 5117 is fairly normal, certainly not expected from a Peimbert type I PN. The mass of the CSPN of IC 5117 is too low for a Peimbert's Type I PN.

The VLA-6 cm continuum observation by Kwok (1995) shows that IC 5117 has a smooth brightness distribution, and its is slightly extended in the E-W direction. Although the structure of IC 5117 is unresolved, and it may be bipolar in the first approximation (Rudy et al. 2001), it may, in fact, have a much more complicated morphology: the diagnostics indicate that the nebula is inhomogeneous, with perhaps as high density as $N_{\epsilon} = 100\,000$ cm^{-3} and perhaps as low as 30 000 – 40 000 cm^{-3}. However, our model and diagnostic analyses show the nebular physical condition can be successfully represented by a homogeneous shell with $N_H = 80\,000$ cm^{-3}. The model predictions are in general successful. The electron temperatures indicated by the diagnostics are relatively high, and this can be modeled with a CSPN T_{eff} of about 120 000 K. Diagnostics and models suggest a relatively high excitation, and the models also predict higher excitation temperatures, e.g. in [O II], [O III], and [Ar III]. Since detailed images are not available, constructing a sophisticated composite model would be too hasty at this stage. However, one must certainly introduce a refinement in the theoretical model construction, as soon as the high spatial resolution (sub-arc-second scale) imaging becomes available in the future.

We express our gratitude to the technical staff of Lick Observatory, who helped us secure these data. We also acknowledge Dr. André B. Fletcher for his careful review of this paper; and Dr. Lauren Likkel for her measurements of all the near-UV lines from the green tube ITS data. This research was supported by the KRF grant No. 2000-015-DP0445, by the Korea MOST Grant No. Star 01-2-500-00, by the KOSEF Grant No. 2000-1-113-001-5, and by STScI Grant No. AR 06372-01 95A.

REFERENCES

Aaquist, O. B., & Kwok, S. 1990, A&AS, 84, 229

Acker, A., Ochsenbein, F., Stenholm, B., Tylenda, R., Marcout, J., & Schohn, C., 1992, Strasbourg -ESO Catalogue of Galactic Planetary Nebulae, Garchung bei Munchen, European Southern Observatory

Aller, L. H., 1984, Physics of Thermal Gaseous Nebulae, (Dordrecht: Reidel Publishing Company)

Aller, L. H., & Czyzak, S. J. 1983, ApJS, 51, 211 (AC83)

Aller, L. H., & Czyzak, S. J. 1979, Ap&SS, 1979, 62, 397 (AC79)

Aller, L. H., & Liller W., 1968, in Middlehurst B.M. and Aller, L.H., eds, Nebulae and Interstellar Matter, University of Chicago Press, Chicago, ch. 9, p498

Beck, S.C. Lacy, J.H., Townes, C.H., Aller, L.H., Gerballe, T.R. & Baas, F. 1981, ApJ, 249, 592

Greig, W. E. 1972 A&A, 18, 70

Gussie, G. T., & Taylor, A. R. 1995, MNRAS, 273, 801

Grevesse, N., & Noels, A. 1993, in Origin and Evolution of Elements, eds. Prantzos, N., Vangioni-Flam, E. Casse, M. (Cambridge Univ. Press, Cambridge, U.K.), 15

Herrick, S., 1935, Lick Obs. Bull., 17, 85

Hubeny, I. 1988, Computer Phys. Comm., 52, 103

Huggins P. J., & Healy, A. P. 1989, ApJ, 346, 201

Hyung, S. 1994, ApJS, 90, 119

Hyung, S., & Aller, L. H., 1996, MNRAS, 278, 551

Hyung, S., Aller, L. H., Feibelman, W. A., & Lee, W.-B. 2001, AJ, in press

Hyung, S., Aller, L. H., Feibelman, W. A., Lee, W.-B., & de Koter, A. 2000, MNRAS, 318, 77

Keenan, F. P., Aller, L. H., Ramsbottom, C. A., Bell, K. L., Crawford, F. L., & Hyung, S. 2000, Proc. Natl. Acad Sci. USA, 97, 4551

Keenan, F. P., Aller, L. H., Bell, K. L., Crawford, F. L., Feibelman, W. A., Hyung, S., McKenna, F. C., & McLaughlin, B. M. 1999, MNRAS, 304, 27

Keenan, F. P., McKenna, F. C., Bell, K. L., Ramsbottom, C. A., Wickstead, A. W., Aller, L. H., & Hyung, S. 1997, ApJ, 487, 457

Keenan, F. P., Aller, L. H., Bell, K. L., Hyung, S., McKenna, F. C., & Ramsbottom, C. A. 1996, MNRAS, 281, 1073

Köppen, J., & Tarafdar, S. P., 1978, A&A, 69, 363

Kingsburgh, R. L., & Barlow, M., J., 1994, MNRAS, 271, 257

Kwok, S. 1985, AJ, 90, 49

Likkel, L., & Aller, L. H. 1986, ApJ, 301, 825 (LA86)

Mamon, G. A., Glassgold, A. E., & Huggins, P. J. 1988, ApJ, 328, 797

Miranda, L. F., Torrelles, J. M., & Eiroa, C. 1995, ApJ, 446, L39

Moore, C. E. 1993, in J. W. Gallagher, ed., 'Tables of Spectra of H, C, N, and O, atoms and ions', CRC press, London

Moore, C. E. 1974, A Multiplet Table of Astrophysical Interest, National Bureau of Standards, No.40

Peimbert, M., Luridiana, V., & Torres-Peimbert, S. 1995, RMxA&A, 31, 147

Rudy, R. J., Lynch, D. K., Mazuk, S., Puertter, R. C., & Dearborn, D. S. P. 2001, AJ, 121, 362

Seaton, M. J. 1979, MNRAS, 187, 73P

Schönberner, B. 1983, ApJ, 272, 708

Zhang, C. Y. 1995, ApJS, 98, 659

Zhang, C. Y., & Kwok, S. 1992, ApJ, 385, 255

This preprint was prepared with the AAS LaTeX macros v5.0.

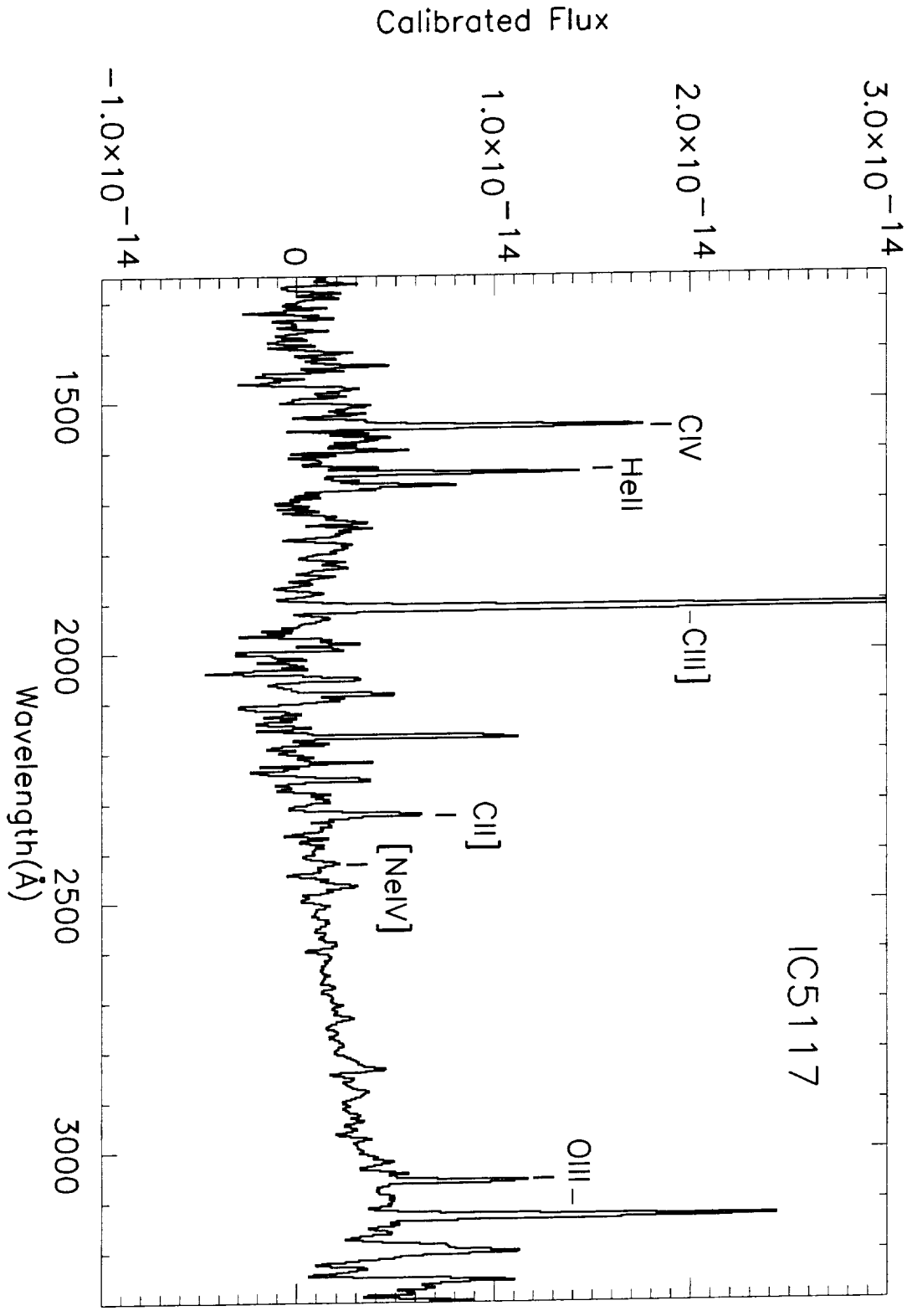

Fig. 1.— The Ultraviolet Spectrum of IC 5117 (extinction correction not applied in this diagram). Although the baseline is below the zero, the flux measurement can be done, correctly (flux unit is erg cm^{-2} s^{-1} $Å^{-1}$). Plot was smoothed by a three point running average.

Fig. 1. — The Ultraviolet Spectrum of IC 5117 (extinction correction not applied in this diagram). Although the baseline is below the zero, the flux measurement can be done, correctly (flux unit is erg cm^{-2} s^{-1} $Å^{-1}$). Plot was smoothed by a three point running average.

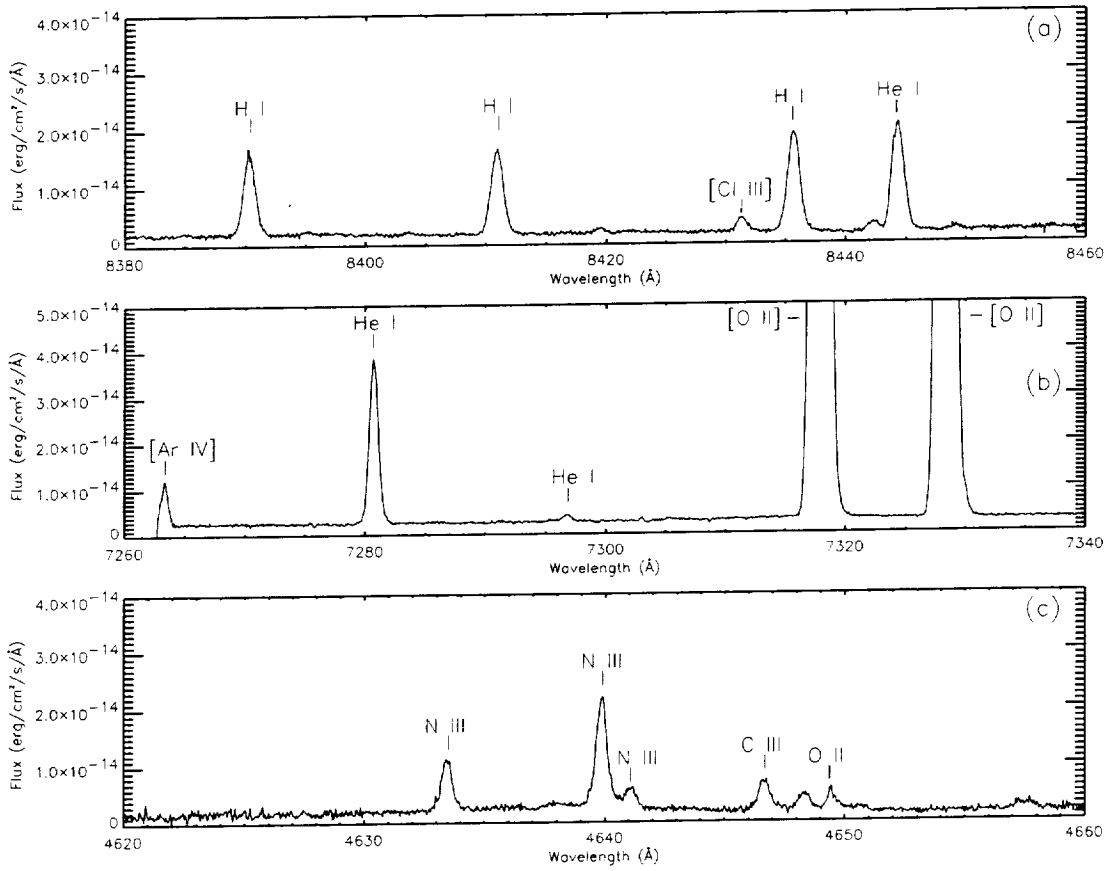

Fig. 2.— Plot of the HES spectrum of IC 5117 — (a) 8380–8460Å, (b) 7260–7340Å, (c) 4620–4660Å. Radial velocity and interstellar extinction corrections are not applied to this spectral scan.

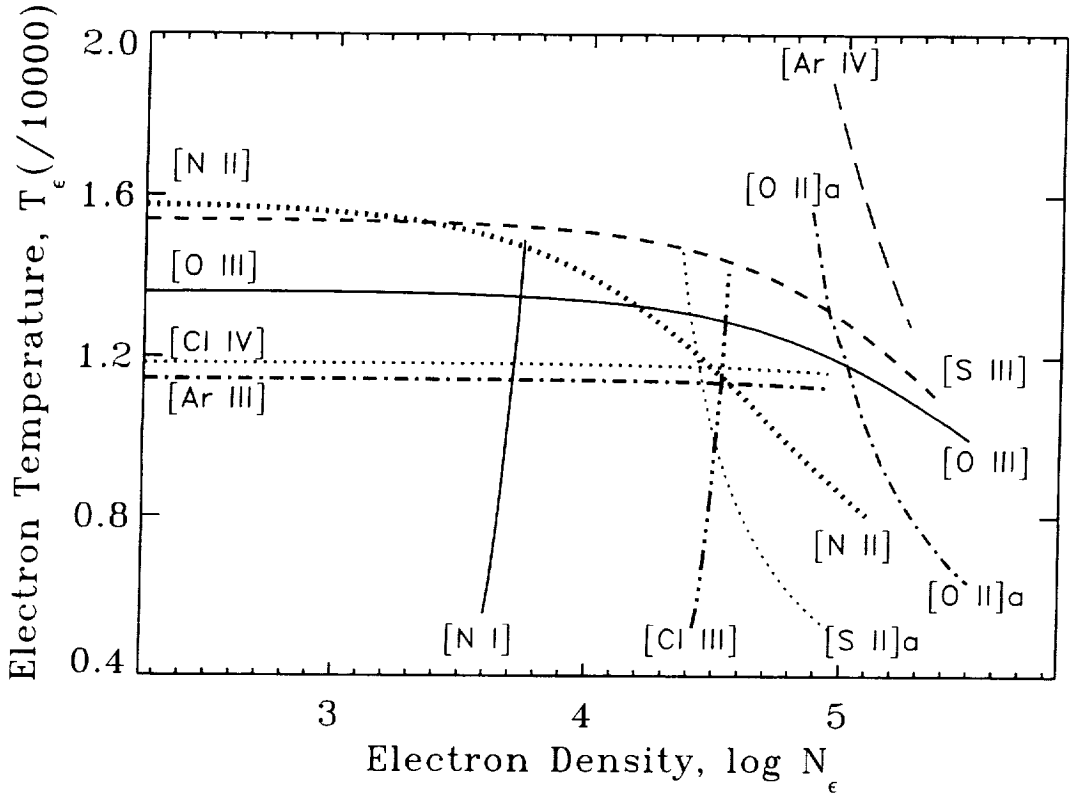

Fig. 3.— Diagnostic diagram for IC 5117 — T_ϵ vs. log N_ϵ. Here [O II]a and [S II]a refer to the transauroral to the nebular transition. These diagnostics are from lines involving p^2 and p^4 electrons. See Table 5 and text for additional diagnostics involving p^3 electrons.

Table 1. Some basic data for IC 5117 (PN G 089.8–05.1).

Basic Data
$\alpha = 21^h32^m30\overset{s}{.}9$, $\delta = 44°35'47''(2000)$,
Diameter $\simeq 1.2'' - 1.5''$; log F(Hβ) = -11.37 $\pm$ 0.01 [erg cm^{-2} s^{-1}]
Excitation class: 6.0
Radial Velocity = -26.1 ± 1.3 km s^{-1}; -38.69$\pm$0.70 km s^{-1} (this paper)
Expansion velocity = 16.5 & 21.5 km s^{-1} ([O III] & [N II], respectively)
Central star: $m_B = 17.5$, $m_V = 16.7$, WR
T($\star$) = 120 000 K (this paper)

References. — These data are from Acker et al. (1992), unless otherwise indicated.

Table 2. *IUE* spectral line intensity.

λ(obs)	λ(rest)	Ion	k_λ[a]	Intensity	Flux
1251.89	1238/40	N v	1.606	33	1.2:
1426.54	1440.36	C iv?	1.283	30	2.8
1548.91	1548/50	C iv	1.184	127	16.1
1573.76	1574.80	[Ne v]	1.168	23	3.0
1596.42	1596.37	C iv?	1.156	16	2.2
1641.08	1640.39	He ii	1.136	59	8.6
1665.88	1661/66	O iii]	1.128	38	5.7
1715.52	1718	N iv	1.119	15	2.3
1751.66	1746/70	N iii]	1.120	12	1.9
1880.82	1882/92	Si iii]	1.193	8.1	1.0
1908.88	1907/09	C iii]	1.228	418	46.4
2323.52	2325/29	C ii]	1.360	83	6.2
2340.85	2334-50	Si II]	1.315	41	3.5
2385.21	2385	He ii	1.204	23	2.8
2421.56	2422/24	[Ne iv]	1.121	11	1.7
2466.76	2470.33	[O ii]	1.031	13	2.6
2832.52	2829	He i	0.622	5.8	3.9
3022.15	3023	O iii	0.507	4.1	3.9
3059.09	3047.13	O iii	0.489	5.6	5.6
3066.78	063/71	[N ii]	0.485	4.7	4.8
3129.78	3232.90	O iii	0.456	9.5	10.5
3199.40	1640.39	He ii	0.426	6.1	7.3

[a] the extinction parameter according to Seaton (1979)

Note. — The UV fluxes in col. (6) are line intensities in units of 10^{-14} erg cm^{-2} s^{-1} Å^{-1}, and the intensities in col. (5) are given based on the scale of I(Hβ) = 100; the interstellar extinction corrections are made assuming $C = 1.29$ [or E(B-V)=0.88]. Colon for fluxes means the estimated error is large, ±40%, while others are ±15%. Only *IUE* Spectra SWP 31825 (150min, 1987 Sep 11) and LWP 05884 (295min, 1985 May 2) were measured in deriving these results.

Table 3. Image tube scanner observation of IC 5117.

λ(obs)	Ion	k_λ	Intensity	Flux	Remarks
3299.00	O III	0.387	0.548	0.74	B
3312.00	O III	0.383	1.08	1.48	B
3317.36	line?	0.381	1.24	1.71	
3341.00	O III	0.372	1.81	2.56	B
3428.00	O III	0.343	0.669	1.03	B
3444.00	O III	0.338	3.22	5.04	B
3512.00	He I	0.317	0.145	0.24	
3530.00	He I	0.311	0.123	0.21	
3554.00	He I	0.304	0.278	0.48	
3587.00	He I	0.295	0.300	0.53	
3613.00	He I	0.288	0.148	0.27	
3634.00	He I	0.282	0.340	0.63	
3679.99	H I	0.270	0.103	0.20	
3683.38	H I	0.269	0.167	0.32	
3687.39	H I	0.268	0.247	0.48	
3692.23	H I	0.266	0.388	0.75	
3697.96	H I	0.265	0.500	0.97	
3727.00	[O II]	0.265	14.7	28.5	
3871.70	H I	0.227	95.2	207	

Note. — ITS measurements by Likkel: 'B' in the remarks column, show lines from the Bowen fluorescent mechanism (see Likkel & Aller 1986, LA86). Interstellar extinction corrected intensities are given on the scale of I(Hβ) = 100 ($C = 1.29$), while fluxes are given in units of 10^{-14}erg cm^{-2} s^{-1}.

Table 4. Optical Spectrum of IC 5117.

λ(obs)	λ(rest)	Ion	Mult.	k_λ	Int(HES)	Flux(HES)	RMS
3703.81	3703.86	H I	H16	0.272	1.304	0.54	26%
3712.04	3711.97	H I	H15	0.269	1.557	0.65	39%
	3721.94	H I	H14				
3721.87	3721.83	[S III]	(2F)	0.267	2.694	1.14	6%
3726.03	3726.03	[O II]	(1F)	0.266	8.666	3.68	2%
3728.75	3728.82	[O II]	(1F)	0.265	2.798	1.19	4%
3734.39	3734.37	H I	H13	0.263	2.084	0.89	
3750.16	3750.15	H I	H12	0.259	2.570	1.11	6%
3754.73	3754.67	O III	(2)	0.258	0.375	0.16	7%
3759.92	3759.81	O III	(2)	0.256	0.991	0.43	11%
	3771.08	N III	(4)				
3770.85	3770.63	H I	H11	0.253	3.300	1.46	18%
3797.90	3797.90	H I	H10	0.246	4.110	1.86	4%
3819.63	3819.61	He I	(22)	0.241	0.822	0.38	18%
3835.40	3835.39	H I	H9	0.236	5.650	2.64	22%
3858.99	3858.07	He II#	4-17	0.230	0.226	0.11	51%
3868.91	3868.71	[Ne III]	(1F)	0.228	103.8	49.77	7%
3888.96	3889.05	H I	H8	0.223	11.48	5.60	11%
3964.75	3964.73	He I	(5)	0.204	0.604	0.31	
3967.49	3967.41	[Ne III]	(1F)	0.203	42.64	22.13	10%
3970.09	3970.07	H I	Hε	0.203	13.30	6.92	23%
4009.43	4009.27	He I	(55)	0.193	0.215	0.12	2%
4026.16	4026.36	He I	(18)	0.189	2.214	1.20	2%
4047.09	4047.80	O II#		0.185	0.292	0.16	
4068.63	4068.60	[S II]	(1F)	0.180	3.030	1.70	4%
4076.29	4076.35	[S II]	(1F)	0.178	1.130	0.64	2%
4097.38	4097.31	N III	(1)	0.173	1.102	0.63	5%
4099.97	4100.04	He II	(4-12)	0.172	0.134	0.08	
4101.78	4101.76	H I	Hδ	0.172	25.70	14.76	3%
4103.42	4103.37	N III	(1)	0.172	0.502	0.29	7%
	4121.46	O II	(19)				
4120.93	4120.81	He I	(16)	0.168	0.280	0.16	35%
	4143.77	O II	(106)				

Table 4—Continued

λ(obs)	λ(rest)	Ion	Mult.	k_λ	Int(HES)	Flux(HES)	RMS
4143.72	4143.76	He I	(53)	0.163	0.287	0.17	6%
4161.97	4162.86	C III#	(21)	0.159	0.165	0.10	10%
4187.00	4186.90	C III	(18)	0.154	0.196	0.12	13%
4199.93	4199.83	He II	(4-11)	0.152	0.222	0.14	11%
4267.14	4267.18	C II	(6)	0.141	0.483	0.31	12%
4338.70	4338.67	He II	(4-10)	0.129	0.308	0.20	17%
4340.61	4340.47	H I	Hγ	0.129	46.50	30.69	5%
4363.20	4363.21	[O III]	(2F)	0.124	19.72	13.24	5%
4373.83	4371.59	C II#	(45)	0.121	0.537	0.36	11%
4387.91	4387.93	He I	(51)	0.117	0.580	0.40	4%
4437.49	4437.55	He I	(50)	0.104	0.123	0.09	1%
4471.48	4471.48	He I	(14)	0.095	5.295	3.90	9%
4541.61	4541.59	He II	(9)	0.077	0.404	0.31	4%
4570.98	4571.00	Mg I]	(1)	0.070	0.504	0.40	8%
4634.13	4634.16	N III	(2)	0.054	0.608	0.51	8%
4640.56	4640.64	N III	(2)	0.053	1.282	1.08	5%
4641.82	4641.81	N III	(2)	0.053	0.183	0.15	
4647.40	4647.40	C III	(1)	0.051	0.436	0.37	
4649.05	4649.14	O II	(1)	0.051	0.242	0.21	2%
4650.23	4650.16	C III	(1)	0.050	0.219	0.19	5%
	4658.64	C IV	(8)				
4658.21	4658.10	[Fe III]	(3F)	0.049	0.152	0.13	5%
4685.71	4685.68	He II	(3-4)	0.042	9.439	8.24	3%
4711.34	4711.34	[Ar IV]	(1F)	0.036	1.129	1.00	15%
4713.11	4713.14	He I	(12)	0.036	0.778	0.69	17%
4725.58	4725.62	[Ne IV]	(1F)	0.033	0.108	0.10	14%
4740.40	4740.20	[Ar IV]	(1F)	0.029	4.722	4.30	11%
4789.49	4789.45	[F II]?		0.018	0.040	0.04	
4811.79		line?		0.012	0.056	0.05	15%
4859.45	4859.32	He II	(4-8)	0.000	0.436	0.44	8%
4861.51	4861.33	H I	Hβ	0.000	100.00	100.00	5%
4880.94	4881.11	[Fe III]	(2F)	-0.005	0.071	0.07	
4921.80	4921.93	He I	(48)	-0.014	0.798	0.84	7%

Table 4—Continued

λ(obs)	λ(rest)	Ion	Mult.	k_λ	Int(HES)	Flux(HES)	RMS
4931.05	4931.30	[O III]	(1F)	-0.017	0.166	0.18	4%
4948.71	4948.54	[Fe III]		-0.021	0.159	0.17	2%
4958.89	4958.92	[O III]	(1F)	-0.023	395.0	425.6	3%
4996.23	4996.29	†		-0.032	0.449	0.50	15%
5007.11	5006.84	[O III]	(1F)	-0.034	1346.4	1503.1	2%
5041.02	5041.06	Si II	(5)	-0.041	0.207	0.24	18%
5047.62	5047.74	He I	(47)	-0.043	0.095	0.11	10%
	5056.35	Si II	(5)				
5056.11	5056.02	Si II	(5)	-0.045	0.194	0.22	6%
	5121.82	C II	(2)				
5121.42	5121.69	C II	(12)	-0.058	0.039	0.05	14%
5131.02	5131.41	C III	5g-7h	-0.060	0.080	0.10	10%
	5146.06	O I?	(28)				
5145.63	5145.77	[Fe VI]	(2F)	-0.063	0.024	0.03	7%
5176.48	5176.40	[Fe VI]	(2F)	-0.070	0.025	0.03	23%
5191.52	5191.80	[Ar III]	(3F)	-0.073	0.156	0.20	4%
5197.66	5197.90	[N I]	(1F)	-0.074	0.151	0.19	
5200.03	5200.26	[N I]	(1F)	-0.074	0.088	0.11	2%
5270.46	5270.40	[Fe III]	(1F)	-0.089	0.084	0.11	11%
5323.23	5323.30	[Cl IV]	(3F)	-0.100	0.044	0.06	1%
5342.10	5342.56	C II		-0.104	0.046	0.06	12%
5345.77	5345.90	[K IV]	(1F)	-0.105	0.129	0.18	8%
	5412.00	[Fe III]	(1F)				
5411.51	5411.52	He II	(2)4-7	-0.118	0.922	1.35	1%
5461.84	5462.62	N II	(29)	-0.128	0.215	0.33	12%
5517.65	5517.71	[Cl III]	(1F)	-0.139	0.142	0.22	11%
5537.61	5537.88	[Cl III]	(1F)	-0.143	0.433	0.69	
5577.52	5577.34	[O I]	(3F)	-0.152	0.139	0.23	8%
5592.07	5592.37	O III	(5)	-0.155	0.036	0.06	
5613.50	5614.7	[Ca VII]#	?	-0.160	0.021	0.04	4%
5631.06	5631.07	[Fe VI]		-0.164	0.018	0.03	11%
5659.98	5660.20	C IV	(1)	-0.170	0.014	0.02	7%
5666.37	5666.64	N II	(3)	-0.172	0.014	0.03	3%

Table 4—Continued

λ(obs)	λ(rest)	Ion	Mult.	k_λ	Int(HES)	Flux(HES)	RMS
5680.13	5679.56	N II	(3)	-0.175	0.038	0.07	30%
5708.64	5710.76	N II#	(3)	-0.181	0.026	0.05	28%
5754.55	5754.64	[N II]	(3F)	-0.191	2.458	4.69	4%
5801.55	5801.51	C IV	(1)	-0.201	0.060	0.11	11%
5811.96	5811.98	C IV	(1)	-0.203	0.035	0.07	8%
5815.54	5815.97	†		-0.204	0.022	0.04	12%
5820.23	5820.43	He II	(5-34)	-0.205	0.010	0.02	24%
5861.56	5863.0	[Mn V]		-0.213	0.040	0.08	17%
5867.76	5867.82	He II+?	Pf29	-0.214	0.160	0.32	1%
5875.57	5875.67	He I	(11)	-0.216	15.16	30.41	6%
5885.42	5885.90	†		-0.218	0.062	0.12	24%
5912.98	5913.24	He II	Pf26	-0.223	0.020	0.04	40%
	5931.79	N II	(28)				
5931.69	5931.83	He II	Pf25	-0.226	0.025	0.05	10%
5952.64	5952.93	He II	Pf24	-0.229	0.021	0.04	20%
6004.40	6004.72	He II	Pf22	-0.238	0.028	0.06	7%
6024.42	6024.15	P II?	(5)	-0.241	0.010	0.02	
6036.58	6036.78	He II	Pf21	-0.243	0.020	0.04	7%
	6046.46	O I	(22)				
6046.14	6046.26	O I	(22)	-0.245	0.034	0.07	12%
6073.74	6074.19	He II	Pf20(8)	-0.249	0.030	0.07	16%
6101.50	6101.80	[K IV]	(1F)	-0.254	0.329	0.74	13%
6118.47	6118.26	He II	Pf19	-0.257	0.019	0.04	4%
6138.94	6138.98	S II?	(63)	-0.260	0.016	0.04	6%
6156.94	6156.6	C III?	(13)	-0.263	0.023	0.05	13%
6161.35	6161.60	[Cl II]		-0.263	0.016	0.04	13%
6165.41	6166.20	[Mn V]#		-0.264	0.019	0.05	1%
6170.49	6170.69	He II	Pf18	-0.265	0.036	0.09	24%
6218.42	6218.6	[Mn V]		-0.272	0.013	0.03	16%
6231.35	line?			-0.274	0.013	0.03	31%
6233.60	6233.82	He II	Pf17(7)	-0.275	0.035	0.09	11%
6300.00	6300.30	[O I]	(1F)	-0.285	6.940	17.38	5%
6312.02	6312.10	[S III]	(3F)	-0.287	2.666	6.71	7%

Table 4—Continued

λ(obs)	λ(rest)	Ion	Mult.	k_λ	Int(HES)	Flux(HES)	RMS
6346.62	6347.09	Si II	(2)	-0.292	0.055	0.14	5%
6363.27	6363.78	[O I]	(1F)	-0.294	2.291	5.92	6%
6370.93	6371.36	Si II	(2)	-0.295	0.097	0.25	8%
6393.80	6393.62	[Mn V]		-0.299	0.042	0.11	2%
6406.09	6406.38	He II	Pf15(7)	-0.300	0.056	0.15	5%
6462.05	6461.95	C II		-0.309	0.059	0.16	12%
6515.55	line?			-0.316	0.019	0.05	2%
6527.62	6527.23	[N II]		-0.318	0.066	0.18	5%
6544.48	6544.50	†		-0.320	0.079	0.22	5%
6547.90	6548.03	[N II]	(1F)	-0.321	14.18	41.98	2%
6559.81	6560.10	He II	(4-6)	-0.322	1.478	4.18	4%
6562.46	6562.82	H I	Hα	-0.323	283.92	803.5	9%
6577.48	6578.03	C II	(2)	-0.325	0.263	0.75	7%
6580.46	line?			-0.325	0.053	0.15	6%
6582.94	6583.45	[N II]	(1F)	-0.326	47.91	144.2	6%
6601.18	6601.10	[Fe VII]	(1F)	-0.328	0.035	0.10	17%
6678.88	6678.15	He I	(46)	-0.338	3.275	9.75	4%
6683.61	6683.15	He II	Pf13(7)	-0.339	0.059	0.18	15%
6715.89	6716.47	[S II]	(2F)	-0.343	0.897	2.71	1%
6730.26	6730.85	[S II]	(2F)	-0.345	2.058	6.25	5%
6743.84	line?			-0.346	0.031	0.09	3%
6780.04	6780.27	C II	(14)	-0.351	0.027	0.08	16%
6787.06	6787.09	C II	(14)	-0.351	0.017	0.05	22%
6791.09	6791.30	C II	(14)	-0.352	0.017	0.05	35%
6794.52	6795.00	[K IV]	(1F)	-0.352	0.069	0.21	20%
6890.37	6890.88	He II	Pf12(7)	-0.363	0.077	0.25	5%
6894.85	6895.29	O II?	(45)	-0.364	0.035	0.11	4%
6978.44		line?		-0.373	0.035	0.12	
7001.66	7002.13	O I	(21)	-0.376	0.036	0.12	16%
7005.44	7005.70	[Ar V]	(1F)	-0.376	0.297	1.00	1%
7064.70	7065.28	He I	(10)	-0.383	10.30	35.40	
7135.28	7135.78	[Ar III]	(1F)	-0.390	16.80	59.16	4%
7154.34	7155.14	[Fe II]#	(14F)	-0.393	0.033	0.12	13%

Table 4—Continued

λ(obs)	λ(rest)	Ion	Mult.	k_λ	Int(HES)	Flux(HES)	RMS
7159.86	7160.5	He I#		-0.393	0.029	0.10	7%
7170.07	7170.62	[Ar IV]	(2F)	-0.394	0.290	1.03	3%
7178.57	7177.52	He II#	?	-0.395	0.104	0.37	11%
7230.61	7231.12	C II	(3)	-0.401	0.093	0.34	2%
7236.44	7236.19	C II	(3)	-0.401	0.403	1.47	4%
7253.64	7254.38	O I#	(20)	-0.403	0.036	0.13	5%
7262.38	7262.96	[Ar IV]	(2F)	-0.404	0.239	0.88	
7281.94	7281.35	He I	(45)	-0.406	0.803	2.97	8%
7297.84	7298.05	He I	(1/9)	-0.407	0.031	0.11	22%
7319.37	7319.40	[O II]	(2F)	-0.410	8.800	32.96	5%
7329.54	7329.90	[O II]	(2F)	-0.411	7.692	28.91	4%
7378.17	7377.83	[Ni II]	(2F)	-0.416	0.011	0.04	
7451.81	7452.5	[Fe II]#	(14F)	-0.423	0.013	0.05	7%
7468.05	7468.29	N I	(3)	-0.424	0.014	0.06	5%
7499.43	7499.84	He I	(1/8)	-0.427	0.047	0.19	18%
7529.64	7530.83	[Cl IV]	(1F)	-0.430	0.422	1.69	9%
7534.11	7534.83	Fe II#	?	-0.431	0.027	0.11	1%
7592.49	7592.74	He II	Pf10(6)	-0.436	0.200	0.81	21%
7750.41	7751.43	[Ar III]#	(1F)	-0.451	4.282	18.32	6%
7815.46	7816.16	He I	(69)	-0.457	0.080	0.35	10%
7821.69	7821.47	S II?	(31)	-0.457	0.042	0.18	12%
7876.96	7875.99	[P II]#	(3F)	-0.462	0.056	0.25	2%
8044.96	8046.27	[Cl IV]#	(1F)	-0.477	0.939	4.37	5%
8186.90	8184.81	N I#	(2)	-0.488	0.015	0.07	21%
8195.70	8196.48	C III#	(43)	-0.489	0.316	1.53	8%
8203.01	8203.9	He I	(4/14)	-0.490	0.016	0.08	16%
8237.07	8236.78	He II	Pf9	-0.492	0.311	1.52	1%
8252.08	8252.50	H I	P39	-0.494	0.041	0.20	15%
8254.58	8255.15	H I	P38	-0.494	0.063	0.31	
8257.53	8257.86	H I	P37	-0.494	0.051	0.25	9%
8260.70	8260.94	H I	P36	-0.494	0.085	0.42	7%
8263.80	8264.29	H I	P35	-0.495	0.090	0.44	2%
8267.20	8267.94	H I	P34	-0.495	0.083	0.41	10%

Table 4—Continued

λ(obs)	λ(rest)	Ion	Mult.	k_λ	Int(HES)	Flux(HES)	RMS
8271.04	8271.93	H I	P33	-0.495	0.090	0.44	
8275.43	8276.31	H I**	P32	-0.495	0.105	0.52	4%
8280.24	8281.12	H I**	P31	-0.496	0.120	0.60	8%
8285.42	8286.43	H I#	P30	-0.496	0.147	0.73	10%
8291.17	8292.31	H I#	P29	-0.497	0.154	0.76	15%
8297.83	8298.84	H I#	P28	-0.497	0.173	0.86	11%
8305.15	8306.12	H I**	P27	-0.498	0.127	0.63	6%
8311.31		line?		-0.498	0.047	0.23	6%
8313.27	8314.26	H I#	P26	-0.498	0.181	0.90	2%
8322.62	8323.43	H I	P25	-0.499	0.194	0.97	5%
8333.16	8333.78	H I	P24	-0.500	0.274	1.37	12%
8343.04	8342.2?	He I#	(4/12)	-0.502	0.054	0.27	4%
8346.34	8345.55	H I	P23	-0.502	0.248	1.25	6%
	8359.66	He I					
8359.18	8359.01	H I	P22	-0.504	0.247	1.26	5%
8361.82	8361.60	He I	(1/6)	-0.504	0.124	0.63	6%
8374.11	8374.48	H I	P21	-0.506	0.261	1.34	12%
8391.55	8392.40	H I#	P20	-0.509	0.337	1.74	3%
8404.98	8405.80	C III#	6f-8g	-0.511	0.013	0.07	33%
8412.22	8413.32	H I#	P19	-0.512	0.366	1.91	1%
8421.30	8420.97	O I	(54)	-0.514	0.022	0.11	3%
8432.63	8433.85	[Cl III]#	(3F)	-0.515	0.052	0.27	6%
8436.96	8437.96	H I#	P18	-0.516	0.412	2.17	7%
8443.57	8444.4	He I#	(4/11)	-0.517	0.025	0.13	
8445.59	8446.48	O I#	(4)	-0.517	0.424	2.25	5%
8450.47	8451.55	S I#	(14)	-0.518	0.025	0.13	18%
8468.17	8467.26	H I	P17	-0.521	0.453	2.43	20%
8481.23	8481.16	[Cl III]	(3F)	-0.523	0.047	0.25	8%
8486.41	8485.8	He I		-0.524	0.022	0.12	
8488.83	8488.77	He I		-0.524	0.022	0.12	28%
8499.56	8500.00	[Cl III]	(3F)	-0.526	0.049	0.27	4%
8502.00	8502.49	H I	P16	-0.526	0.517	2.82	
8527.91	8528.99	He I#	6/15,10/17	-0.530	0.023	0.13	8%

Table 4—Continued

λ(obs)	λ(rest)	Ion	Mult.	k_λ	Int(HES)	Flux(HES)	RMS
8544.21	8545.38	H I	P15	-0.532	0.673	3.74	15%
8577.93	8578.70	[Cl II]#	(1F)	-0.537	0.195	1.10	18%
8581.53	8581.70	He I	(6/14)	-0.538	0.087	0.49	30%
8599.21	8598.39	H I#	P14	-0.540	0.781	4.46	4%
8617.08	8616.96	[Fe II]	(13F)	-0.543	0.040	0.23	12%
8647.30	8648.26	He I#	(6/13)	-0.547	0.042	0.24	10%
8660.86	8661.40	He II	(6-26)	-0.549	0.039	0.23	7%
8663.85	8665.02	H I#	P13	-0.550	1.046	6.15	14%
8728.03	8727.13	[C I]#		-0.559	0.140	0.85	12%
8734.05	8733.43	He I	(6/12)	-0.560	0.031	0.19	5%
8750.42	8750.48	H I	P12	-0.562	0.984	6.03	5%
8776.14	8776.77	He I	(4/9)	-0.566	0.065	0.40	10%
8788.92	8787.60	[P I]#		-0.568	0.026	0.16	
8797.72	8798.90	He II#	(6-23)	-0.569	0.020	0.13	19%
8844.67	8845.38	He I	(6/11)	-0.575	0.068	0.44	18%
8847.67	8848.05	He I	(7/11)	-0.576	0.035	0.22	7%
8863.84	8862.79	H I	P11	-0.578	1.502	9.68	16%
8926.29	8926.06	Mn I?	(56)	-0.587	0.098	0.65	21%
8929.47	8929.00	He II	(6-21)	-0.587	0.011	0.07	37%
8985.83		line?		-0.595	0.025	0.17	10%
8996.25	8996.99	He I	(6/10)	-0.596	0.079	0.54	22%
8998.45	8999.75	He I#	(7/10)	-0.596	0.063	0.43	6%
9000.79	8999.75	He I#	(7/10)	-0.597	0.043	0.29	27%
9015.42	9014.91	H I	P10	-0.599	1.510	10.40	32%
9062.21	9062.53	C I	(3)	-0.605	0.064	0.45	27%
9067.88	9068.90	[S III]	(1F)	-0.606	22.34	157.4	13%
9122.70	9123.60	[Cl II]#	(1F)	-0.610	0.053	0.38	39%
9209.25	9210.28	He I#	(83),6/9	-0.612	0.111	0.79	39%
9212.03	9212.53	S I?	(1)	-0.612	0.034	0.24	45%
9213.80	9213.24	He I	(7/9)	-0.612	0.037	0.27	38%
9222.03		line?		-0.612	0.054	0.39	40%
9223.84		line?		-0.612	0.038	0.28	47%
9227.66	9227.70	He I	(5/9)	-0.612	3.287	23.66	34%

Table 4—Continued

λ(obs)	λ(rest)	Ion	Mult.	k_λ	Int(HES)	Flux(HES)	RMS
9231.21	9229.02	H I#	P9	-0.612	0.022	0.16	42%
9373.49	9373.28	Ne I	(33)	-0.616	0.162	1.18	50%
9464.32	9463.57	He I	(1/5)	-0.618	0.264	1.94	28%
9515.39	9516.5	He I#	(4/7)	-0.619	0.114	0.84	47%
9524.87	9526.0	He I#	(6/8)	-0.620	0.135	1.00	39%
9529.78	9531.0?	[S III]#	(1F)	-0.620	65.68	484.2	21%
9544.65	9545.97	H I	P8	-0.620	3.140	23.17	42%
9691.00		line?		-0.624	0.086	0.64	15%
9823.23	9824.11	[C I]#	(1F)	-0.627	0.100	0.76	12%
9848.76	9850.24	[C I]#	(1F)	-0.627	0.272	2.06	8%
9902.19	9902.70	[K III]	(1F)	-0.628	0.148	1.12	9%
10026.2	10027.7	He I#	(6/7)	-0.631	0.194	1.48	11%
10029.6	10027.6	He I#	(6/7)	-0.631	0.071	0.54	23%
10043.5	9545.9	He II#	(6-14)	-0.631	0.052	0.40	20%
10047.7	10049.4	H I#	P7	-0.631	4.808	36.81	3%
10125.6	10123.6	He II#	(4-5)	-0.633	0.191	1.47	32%
10321.3	10320.6	[S II]#		-0.637	0.378	2.95	45%
10336.3	10338.8	[S II]#		-0.638	0.249	1.95	47%

† These unidentified lines are seen in other PNe, e.g. IC 4997 and NGC 7662.

? Unlikely identification.

Identification with too large a wavelength discrepancy.

** Lines affected by telluric absorption lines. Some lines may be lost in the telluric absroption region, e.g. 7595 – 7700Å. The spectrum of IC 5117 was not divided by that of a standard star to take out the first order effects of the atmosphere.

References. — See Hyung & Aller (1996) for the identifications and references therein.

Table 5. Diagnostic Line Ratios suitable for fixing N_ϵ, T_ϵ.

Ion	Lines	Ratio	Determines	Remarks
[N I]	I(λ5198)/I(λ5200)	1.72	N_ϵ	
[N II]	I(λ6548 + λ6583)/I(λ5755[a])	25.3	T_ϵ	
[O II]	I(λ3726) / I(λ3729)	3.10	N_ϵ	N/A ?
[O II]	I(λ3726 + λ3729) / I(λ7319/20 + λ7329/30)	0.695	N_ϵ,T_ϵ	[O II]a
[O III]	I(λ4959 + λ5007) / I(λ4363)	88.3	T_ϵ	
[Cl III][a]	I(λ5518) / I(λ5538)	0.328	N_ϵ	
[Cl IV]	I(λ7530 + λ8045) / I(λ5323)	30.9	T_ϵ	
[Ar III]	I(λ7136 + λ7751) / I(λ5191[a])	135.1	T_ϵ	
[Ar IV]	I(λ4740 + λ4711) / I(λ7171)	20.2	N_ϵ,T_ϵ	N/A ?
[S II]	I(λ6716[a] + λ6731) / I(λ4069[a])	0.975	N_ϵ,T_ϵ	[S II]a
[S II]	I(λ6716[a])/ I(λ6731)	0.436	N_ϵ	N/A ?
[S III]	I(λ9069 + λ9531[a])/ I(λ6312)	33.0	T_ϵ	

[a]relatively weak line, or of poor quality.

Note. — N/A ?: diagnostic informations is useless, or not in a reasonable range (due to observational errors, or poor measurements).

Table 6. Model Details for IC 5117.

Parameter	Model B
R_{in}(pc)	0.008
R_{out}(pc)[a]	0.0154 ($\triangle\theta \sim 1.06''$)
N_H(cm^{-3})	80 000
DISTANCE =	3000 pc
M_{dust}/M_{gas} =	0.001
F(Hβ)–obs[b] =	$8.33 \sim 10.7(-11)$ erg cm^{-2} s^{-1}
F(Hβ)–pred =	$9.67(-11)$ erg cm^{-2} s^{-1}
CSPN T($\star$)[c] =	120 000 K (log g = 8.5)
CSPN R($\star$) =	0.16 $R_\odot$ (L($\star$) = 5000 $L_\odot$)
T_ϵ([O II, III, IV])	12 500,11 800,13 500 K
Magnitude	V_{pred} = 15.1 & V_{obs} = 14.0[d]

[a] density bounded.

[b] extinction corrected with $C = 1.29 \sim 1.4$.

[c] Hubeny non-LTE model atmosphere. See text.

[d] corrected with E(B-V)=0.88.

Table 7. Comparison of observed and predicted intensities for IC 5117.

El–ion	λ	I(AC79)[a]	I_{obs}[b]	I(Model-A)	I(Model-B)
He I	5876	14.79	15.16	14.61	15.49
	6678	2.82	3.28	3.72	3.81
	4471	4.36	5.30	5.09	5.41
He II	4686	9.33	9.44	9.99	7.63
	5412	0.74	0.92	0.81	0.64
	1640		[58.8]	68.6	55.3
C II	2325/28		[83.0]	53.0	60.8
	4267	0.43	0.48	0.47	0.27
C III	1907/09		[418.0]	401.2	415.3
C IV	1548/51		[126.9]	209.0	409.9
N II	6584	38.09	50.61	45.85	41.96
	6548	12.88	14.18	15.83	14.49
	5755	2.04	2.46	1.97	3.17
N III	1747-52		[12.4]	17.8	17.5
N IV	1483/86		...	6.51	12.23
O II	3726	11.1[c]	8.67	7.70	7.24
	3729	3.59[c]	2.80	2.77	2.55
	7321/2	6.57[c]	8.80	3.63	7.22
	7332/3	5.73[c]	7.69	2.92	5.80
O III	1660/66		[38.0]	16.6	27.4
	4363	19.95	19.72	13.31	20.17
	4959	524.8	395.0	452.8	481.5
	5007	1479	1346	1304	1387
Ne III	3868	154.9	103.8	132.0	135.5
	3969	61.66	42.64	39.38	40.43
Ne IV	2422/25		[11.1]	3.39	5.56
	4725/27	0.27	0.11	0.03	0.10
S II	4068	3.47	3.03	1.64	3.06
	4076	1.07	1.13	0.55	1.01
	6717	0.58	0.90	0.32	0.30
	6731	1.29	2.06	0.70	0.66
S III	6312	2.04	2.67	2.29	2.31
	9069	...	22.34	33.52	25.26

Table 7—Continued

El–ion	λ	I(AC79)[a]	I_{obs}[b]	I(Model-A)	I(Model-B)
	9531	···	65.68	81.66	61.53
S IV	10.5μm	33.6[d]	···	73.21	31.4
Cl III	5518	0.083	0.14	0.15	0.08
	5538	0.29	0.43	0.50	0.31
Cl IV	7530	0.27	0.42	0.42	0.47
	8046	0.66	0.94	0.97	1.10
Ar III	5193	0.15	0.16	0.14	0.14
	7136	14.13	16.80	16.36	12.41
	7751	3.24	4.28	3.95	3.00
Ar IV	4711	1.84	1.13	2.42	1.86
	4740	5.13	4.72	8.52	8.96
	7238	0.25	···	0.16	0.24
	7263	0.12	0.24	0.17	0.10
	7171	0.16	0.29	0.12	0.20
Ar V	6435	0.03	···	0.12	0.30
	7005	0.16	0.30	0.26	0.64
K IV	6102	0.19	0.33	0.33	0.33
Si III	1883/92		[41.7]	44.66	45.53

[a] Aller & Czyzak (1979, AC79).

[b] [I_{obs}]: Intensities in square brackets are from the low resolution *IUE* data.

[c] Calculated using the HES line ratios. ITS spectral resolution ~2Å.

[d] [S IV] measurement from Beck et al. (1981), and intensity is obtained assuming I(Hβ) = 8.33(-11) erg cm^{-2} s^{-1} [See Table 6].

Table 8. Fractional ionic concentration.

Ion	Wavelength	Intensity	$\frac{N(ion)}{N(H^+)}$	$\Sigma\frac{N(ion)}{N(H^+)}$
He I	6678	3.275	7.84(-2)	
	5876	15.16	8.87(-2)	
He II	4686	9.44	8.13(-3)	
	5412	0.92	5.84(-3)	9.84(-2)
C II	2325/28	83	4.82(-5)	
C III	1907/09	418	3.44(-4)	
C IV	1549/51	127	8.19(-5)	4.74(-4)
N II	6548/84,5755	14.18,47.91,2.46	1.08(-5),1.26(-5),9.07(-6)	
N III	1753–	12	4.54(-5)	5.75(-5)
O I	6300/63	6.94,2.29	6.79(-6),7.04(-6)	
O II	3727/29,7320/30	8.67,2.80,8.80,7.69	3.03(-5),2.78(-5),4.13(-5),6.89(-5) 1.05(-5),0.94(-5),2.76(-5),4.62(-5)[a]	
O III	4957,5007,4363	395,1346,19.7	2.84(-4),3.33(-4),3.36(-4)	3.73(-4)
O III	1660–	38	4.92(-4)[b]	
Ne III	3869/3967	103.8,42.6	4.54(-5),6.26(-5)	
Ne IV	2422–	11	1.27(-5)	6.31(-5)
S II	6717/31,4068	0.90,2.06,3.03	7.23(-7),7.48(-7),2.31(-7)	
S III	6312,9069,9531	2.67,22.34,65.68	3.12(-6),2.26(-6),2.73(-6)	
S IV	10.5μm	33.6	4.26(-6)	7.37(-6)
Ar III	7135,7751,5192	16.8,4.28,0.16	9.81(-7),1.04(-6),8.67(-7)	
Ar IV	4711/40,7263,7171	1.13,4.72,0.24,0.29	5.52(-7),5.01(-7),1.14(-6)[b],1.10(-6)[b]	
Ar V	7006	0.30	3.54(-8)	1.59(-6)
Cl III	5517/37	0.14,0.43	7.59(-8),5.91(-8)	
Cl IV	7530/8045,5323	0.42,0.94,0.044	6.38(-8),6.12(-8),5.90(-8)	1.25(-7)
K IV	6102	0.329	5.94(-8)	5.94(-8)

Table 8—Continued

Ion	Wavelength	Intensity	$\frac{N(ion)}{N(H^+)}$	$\Sigma\frac{N(ion)}{N(H^+)}$
Si III	1882/92	41.7	7.52(-6)	7.52(-6)

[a]derivation with $N_\epsilon = 40\,000$ cm^{-3} and $T_\epsilon = 13\,000$ K (see text).

[b]ignored because of relatively weak line intensities.

Note. — X(-Y) implies X $\times$ 10^{-Y}. Ionic concentrations are derived with $N_\epsilon = 90\,000$ cm^{-3} and $T_\epsilon = 12\,000$ K.

Table 9. Comparison of ICF and Model abundances for IC 5117.

Elem.	$\Sigma\frac{N(ion)}{N(H^+)}$	ICF	N(ICF)	N(Model)	$\triangle$	IC 5117	AC83[a]	Mean[b]	SUN[c]
He I, II	9.84(-2)	1.02	1.00(-1)	9.86(-2)	0.01	0.10	0.11	0.11	0.1
C II, III, IV	4.74(-4)	1.02	4.83(-4)	6.00(-4)	-0.09	5.00(-4)	8.9 (-4)	6.48(-4)	3.55(-4)
N II, III	5.75(-5)	1.92	1.10(-4)	1.40(-4)	-0.10	1.30(-4)	1.31(-4)	1.40(-4)	9.33(-5)
O I, II, III	3.73(-4)	1.04	3.88(-4)	3.75(-4)	0.01	3.80(-4)	3.75(-4)	4.93(-4)	7.41(-4)
Ne III, IV	6.31(-5)	1.02	6.44(-5)	6.50(-5)	-0.00	6.50(-5)	9.31(-5)	1.25(-4)	1.17(-4)
S II, III, IV	7.37(-6)	1.21	8.85(-6)	9.00(-6)	-0.01	8.90(-6)	1.21(-5)	8.08(-6)	1.62(-5)
Ar III, IV, V	1.59(-6)	1.01	1.61(-6)	2.00(-6)	-0.09	1.80(-6)	2.07(-6)	2.42(-6)	3.98(-6)
Cl III, IV	1.25(-7)	1.55	1.94(-7)	1.70(-7)	0.06	1.85(-7)	1.43(-7)	1.66(-7)	3.88(-7)
K IV	5.94(-8)	1.11	6.59(-8)	6.50(-8)	0.00	6.50(-8)	3.3 (-8)	···	1.35(-7)
Si III	7.52(-6)	6.67	5.01(-5)	5.00(-5)	0.00	5.00(-5)	···	···	3.55(-5)

[a] Aller & Czyzak (1983, AC83).

[b] Average (or normal) abundances by Kingsburgh & Barlow (1994) and Aller & Czyzak (1983)

[c] Solar abundances from Grevesse and Noels (1993).

Note. — X1,X2(-Y) implies X1 $\times$ 10^{-Y}, X2 $\times$ 10^{-Y}. All abundances are given relative to $N(H^+)$. $\triangle$: the logarithmic difference, i.e., $\log N$(ICF) $-\log N$(Model), which is less than 0.1 dex for most elements. Our derivation agrees with AC83 to within a factor of 2 (<0.3 dex).